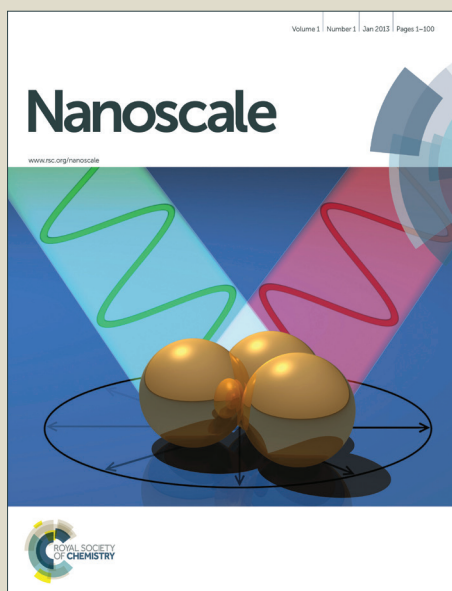


Nanoscale

Accepted Manuscript

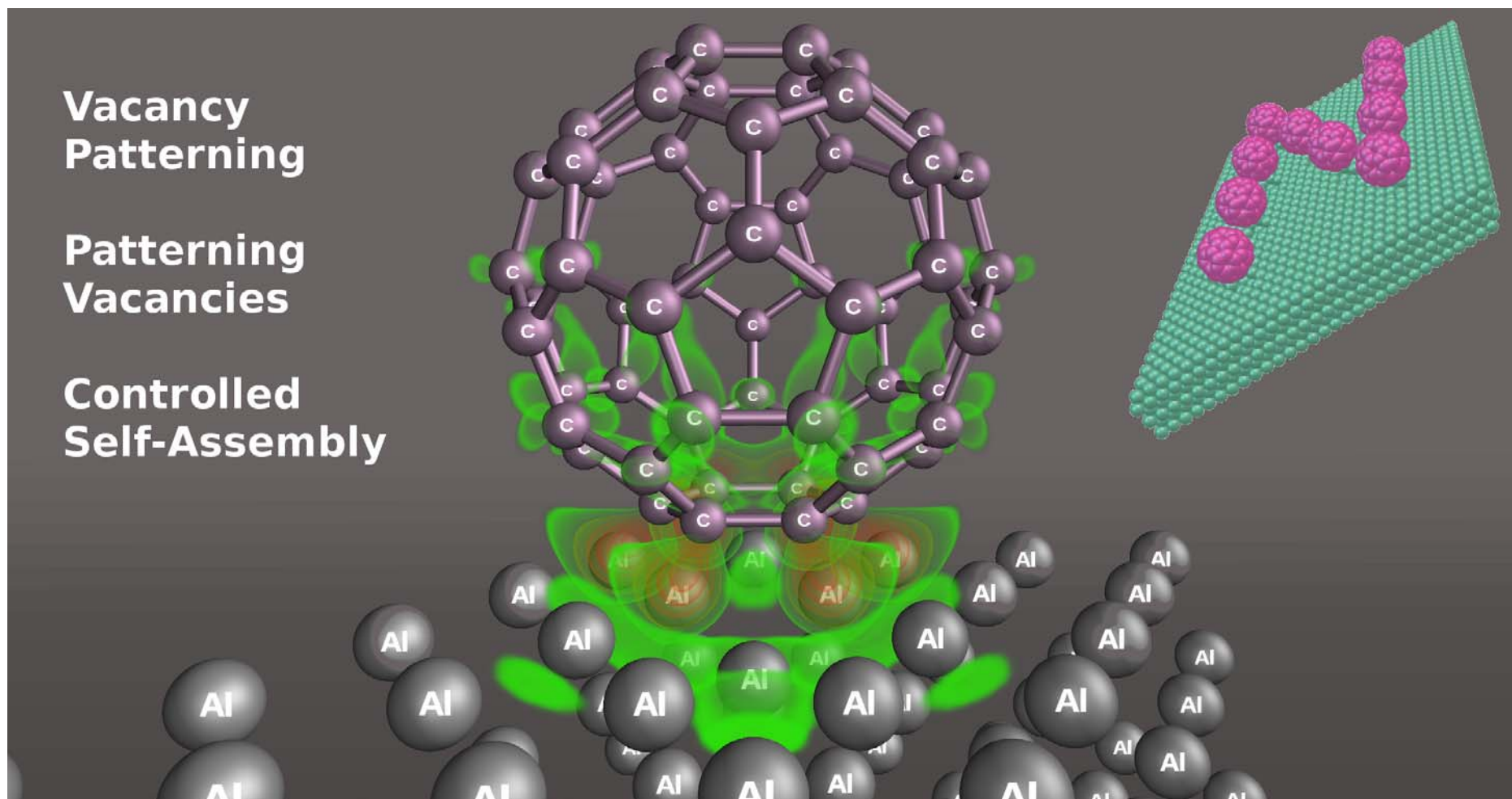


This is an *Accepted Manuscript*, which has been through the Royal Society of Chemistry peer review process and has been accepted for publication.

Accepted Manuscripts are published online shortly after acceptance, before technical editing, formatting and proof reading. Using this free service, authors can make their results available to the community, in citable form, before we publish the edited article. We will replace this *Accepted Manuscript* with the edited and formatted *Advance Article* as soon as it is available.

You can find more information about *Accepted Manuscripts* in the [Information for Authors](#).

Please note that technical editing may introduce minor changes to the text and/or graphics, which may alter content. The journal's standard [Terms & Conditions](#) and the [Ethical guidelines](#) still apply. In no event shall the Royal Society of Chemistry be held responsible for any errors or omissions in this *Accepted Manuscript* or any consequences arising from the use of any information it contains.



Vacancy Patterning and Patterning Vacancies: Controlled Self-Assembly of Fullerenes on Metal Surfaces

Alexander Kaiser^{ab}, Francesc Viñes^b, Francesc Illas^{b*}, Marcel Ritter^c, Frank Hagelberg^d,
Michael Probst^{a*}

^a*Institut of Ion Physics and Applied Physics, University of Innsbruck, Technikerstrasse 25,
A-6020 Innsbruck, Austria*

^b*Departament de Química Física & Institut de Química Teòrica i Computacional
(IQTUCUB), Universitat de Barcelona, c/Martí i Franquès 1, E-08028 Barcelona, Spain*

^c*Institute for Basic Sciences in Engineering Science, University of Innsbruck,
Technikerstrasse 13, A-6020 Innsbruck, Austria*

^d*Department of Physics and Astronomy, East Tennessee State University, Johnson City, TN
37614, USA*

*e-mails: michael.probst@uibk.ac.at; francesc.illas@ub.edu

Abstract

A density functional theory study accounting for van der Waals interactions reveals the potential of metal surface vacancies as anchor points for the construction of user-defined 2D patterns of adsorbate molecules *via* a controlled self-assembly process. *Vice versa*, energetic criteria indicate the formation of regular adsorbate-induced vacancies after adsorbate self-assembly on clean surfaces. These processes are exemplified by adsorbing C₆₀ fullerene on Al(111), Au(111), and Be(0001) surfaces with and without single, triple, and septuple atom pits. An analysis of vacancy-adatom formation energetics precedes the study of the adsorption processes.

Keywords: Adsorption · Self-Assembly · Fullerene · Vacancy Formation · Nanopatterns ·
Metal Surfaces

Introduction

The increasing research interest on Self-Assembled Monolayers (*SAMs*), patterned arrangements typically consisting of organic molecules, is related to their promising applications in biosensors,¹ optoelectronics,² and tribology.³ Typically, such arrangements are studied on metal surfaces, although recent research endeavors have been applied on SAM formation on graphene layers, an appealing field for graphene bandgap engineering,⁴ but also in order to get, for instance, ordered magnetic organic layers.⁵ On the other hand, defined vacancy patterns on surfaces were created, on a nanometer scale, as early as in 2002 within the *millipede project*.⁶ It involved a two-dimensional (2D) array of Atomic Force Microscopy (*AFM*) tips which resembled nm-scale millipedes which imprinted user-defined patterns of vacancies on a given thin polymer surface.

Surface vacancies are particularly attractive adsorption sites for subsequently deposited molecules, given the low-coordination of vacancies neighboring surface atoms, and their concomitant improved chemical activity. When the adsorption of a molecule turns out to be thus strongly enhanced by the presence of a vacancy, as compared to the clean surface, individual population of vacancies can become preferred to molecular clustering, i.e. SAM formation. Thus, a vacancy-determined pattern of adsorbate molecules can be constructed. We call this process Controlled Self-Assembly (*CSA*), and we shall investigate below its feasibility taking fullerene C_{60} adsorption on gold, aluminum, and beryllium surfaces as key example cases.

Another related process is a type of SAM formation which, on the contrary, *induces* the creation of surface vacancies. Conceptually, the fullerenes, first adsorbed on the clean surface, would induce vacancy formation beneath them and reside in their self-made *nests*. Vacancy formation triggered by the adsorption of a molecule or a cluster on a surface is not

rare, and has been observed, for instance, on Pt clusters on CeO₂ substrates.⁷ As far as fullerenes are considered, vacancy incitement in the course of C₆₀ monolayer formation on various surfaces has been investigated by many experimental and theoretical studies.⁸⁻¹⁴ On one hand, these structures remain stable at Room Temperature (RT),¹⁵ and C₆₀ adsorption is found to induce dimple formation on the Au(111) substrate, with well-separated individual C₆₀ nucleation centers for cluster formation upon continued deposition. Vacancies were found to compete with step edges for adsorbates, underlying the importance of under-coordination in the increased adsorbent capacity. On the other hand, Tzeng *et al.* observed that annealing to 750 K desorbs all C₆₀ molecules of Au(111) while preserving the structure of C₆₀.¹⁶ However, vacancy formation was not discussed in their work.¹⁶

The adsorption of C₆₀ on metal surfaces is indeed a topic that has drawn much attention over the last years, and the nature of the C₆₀↔substrate chemical bonding is still a matter of debate. Related research has involved a variety of transition metals (Au,¹⁷⁻²³ Ag,²⁴⁻²⁶ Ni,^{27, 28} Pd,²⁹ Pt,³⁰⁻³⁴ and Cu³⁵⁻⁴⁰) and even few *p*-group metals (Al⁴¹⁻⁴⁴ and Si^{45, 46}), combining experiments and theoretical calculations. The latter mostly rely on Density Functional Theory (DFT), although for such systems the inclusion of a proper description of van der Waals (*vdW*) dispersive forces appears mandatory. Two recent studies of C₆₀ adsorbed on smooth Au(111) and Ag(111) surfaces with and without *vdW* correction revealed a strong covalent, partly ionic interaction of ~1-3 eV strength, where the metal→C₆₀ charge transfer plays a key role.^{17, 25} However, pristine metal surfaces are found to reconstruct when exposed to fullerenes: A clean Au(111) surface tends to adopt a herringbone-structure,^{47, 48} which, as revealed by X-Ray Diffraction (*XRD*) measurements and structural analysis, undergoes at 160 °C a surface transformation accompanied by removal of the herringbone structure and introduction of surface vacancies. Fullerenes were found to reside atop of a regular (2√3×2√3)R30° pattern of vacancies with C-Au distances of 2.49 Å.⁹ These surface

reconstructions, such as vacancy or crater formation, were experimentally observed and confirmed by DFT theory for C_{60} adsorbed on Pt(111),¹³ Ag(111),¹⁴ Al(111),^{43, 44} and Au(110).¹¹

Here we consider representatives and structurally similar surfaces of a noble metal, Au(111), a *p*-group metal, Al(111), and an alkaline earth metal, Be(001). These metals were selected for several different reasons; most of the related literature deals with C_{60} adsorption on Au, which therefore is presented as a good reference system and test field. Secondly, Al is used as electrode material in organic photovoltaics, where it is in contact with the functionalized fullerene Phenyl- C_{61} -Butyric acid Methyl ester (*PCBM*).^{49, 50} Lastly, Be is selected because it exemplifies the field of main-group elements that gain increasing attention. For example, it has been suggested as a potential candidate for walls of future fusion reactors,^{51, 52} and studies of the interaction of carbonaceous materials with beryllium are very rare since experiments with Be need special precautions due to its toxicity. Comparing the energetics of Be and Al in this work is also of interest in this context.

At variance with most of the large amount of work already done in the field, we considered well-separated C_{60} molecules in large unit cells to specifically assess the interaction of C_{60} with the surface, contrary to previous studies dealing with close-packed C_{60} monolayers. Furthermore, our approach explicitly includes vdW forces, which has only been accounted for in one publication of C_{60} adsorption on Au(111) where, however, vacancy formation was not considered.¹⁷ We also analyze vacancy adatom formation energetics, with a subsequent comparison of adsorption energies, charge transfer, and bond nature for C_{60} adsorption on clean surfaces, as well as in single, triple, and septuple atom pits. Energy criteria for vacancy formation inducement and controlled self-assembly are discussed.

Computational Details

All DFT calculations and structural optimizations were carried out using the VASP code.⁵³⁻⁵⁶ A basis set of Plane-Waves (*PW*) was used with a PW kinetic energy cutoff of 415 eV. Valence electrons were described using the Perdew-Burke-Ernzerhof (*PBE*) exchange-correlation functional, whereas core electrons were described by using the Projector Augmented Wave (*PAW*) method. The vdW forces are treated by the long-range correction as proposed by Grimme.^{53, 57-59} Default vdW parameter values were used for C, Al, and Be atoms, whereas for Au atoms we used the values supplied by Amft et al.⁶⁰ Another way to describe surface polarization than with the usual sum of atomic C_6 terms has been proposed by Nguyen et al.⁶¹ The necessary parameterization is out of the scope of the present study, however. For our systems, this would also only minimally influence the final results. A sufficiently accurate \mathbf{k} -point mesh was chosen for all calculations, which happened to be the Γ point for large cells.

A (5×5) unit cell was chosen for the six atomic layer slab model representing the Al(111) and Au(111) surfaces with two frozen and four flexible layers —i.e. (2+4) approximation— and a vacuum thickness of 14 Å, similar to that used previously in related works.²⁵ A larger (8×8) unit cell had to be used for the Be(0001) surface, in order to achieve a large enough separation of C_{60} from its periodic images. The distance between the carbon atoms of C_{60} and their periodic images is in all simulations larger than 7 Å, giving results close to vacuum conditions. One can argue that the vacancies generated by the adsorbed fullerenes (see next section) exhibit a periodicity which is not realistic. However, while this exact situation will hardly be found in experiments, the results are likely to remain unchanged when using even larger supercells able to accommodate two or more fullerenes randomly placed at the surface, provided the distance between the fullerenes is large enough which is the case in the present models. In the direction perpendicular to the surface, the distance

between the topmost carbon atoms and the bottom metal layer of the periodic slab image is always larger than 6.5 Å. To construct input geometries, C₆₀ was manually located above the surface or the center of a vacancy with one of its carbon hexagons pointing downwards at a substantially larger distance than that found in the optimized geometry. During the optimization C₆₀ is allowed to fully relax, as well as the top four surface metal layers.

We first validated our computational settings by optimizing metal lattice constants (a , in case of Be also c) and calculating cohesive energies (CE), work functions (WF) and surface energies (SE). As can be seen in Table 1 we found good agreement with literature (lit.) values. Our resulting optimized lattice constants were adopted throughout this work. Last but not least, molecules were visualized in the *Vish* visualization shell.⁶²⁻⁶⁴ An estimated number of 44 single core wall clock years on Intel Xeon X5650 and similar processors was spent in total for the optimizations.

Table 1: Lattice constants (a , c in Å), cohesive energies (CE in eV), work functions (WF in eV), and surface energies (SE in J/m²) compared with literature data.

	a/c	lit.	CE	lit.	WF	lit.	SE	lit.
Al	4.013	4.04 ⁶⁵	3.73	3.23-4.21 ⁶⁶	4.13	4.24-4.54 ^{67, 68}	1.1	0.94-1.27 ^{68, 69}
Au	4.082	4.079 ⁶⁵	3.74	3.73-3.97 ⁷⁰	5.06	4.83-6.01 ^{68, 71, 72}	1.4	1.25-1.61 ^{68, 73}
Be	2.236/ 3.54	2.282 ⁷⁴ / 3.575 ⁷⁴	3.85	3.32-4.0 ⁷⁵	5.27	4.98-5.62 ⁶⁸	2.1	2.1-2.7 ⁶⁸

Vacancy Formation

First we dealt with the formation of surface vacancies, since they can enhance the binding strength of adsorbed C₆₀ and even lower the total energy of the C₆₀/surface system through surface reconstruction. Often these vacancies are termed pits or craters. Deep pits

with 3 or 7 atom vacancies have shown to increase adsorption energies of the $C_{60}/Au(111)$ system according to DFT calculations without dispersion corrections.¹⁵ Single-atom and regular multi-atom vacancies have been optimized starting from pristine ideal surfaces, from which 1, 3, or 7 (v) atoms have been removed. Three-atom vacancies form a triangular pit, whereas seven-atom vacancies form a hexagonal pit. These structures are similar to those depicted by Tang *et al.*, yet residing in a larger unit cell.¹⁵

The vacancy-adatom formation energy is defined as⁷⁶

$$E_{va}(v) = T(-v) + T(v) - 2 T(0), \quad (1)$$

where $T(\pm v)$ is the total energy of the clean surface $T(0)$, with v additional or $-v$ removed atoms, i.e. $T(-3)$ is the total energy of a surface with a three-atom vacancy, whereas $T(7)$ is the total energy of a surface with seven adatoms. E_{va} is defined as the energy cost of building a vacancy from a clean surface, where the removed atoms attach, as a cluster, to the surface at an infinite distance from the vacancy. Thus the vacancy-adatom formation energy E_{va} can be represented as sum of the adatom formation energy E_{ad} and the vacancy formation energy E_{vac} . Both are defined with reference to the total energy of a bulk atom T_{bulk} :

$$E_{ad}(v) = T(v) - T(0) - v T_{bulk}, \quad (2)$$

$$E_{vac}(v) = T(-v) + v T_{bulk} - T(0). \quad (3)$$

In other words, E_{ad} is the energy required to remove v atoms from the bulk and add them collectively on top of the surface, whereas E_{vac} is the energy gained by removing v atoms from the clean surface and adding them to the bulk reservoir.⁷⁷ The adatom binding energy E_{bad} and the vacancy binding energy E_{bvac} are calculated using the atomic vacuum energy T_{at} as reference energy instead of the bulk value:

$$E_{bad}(v) = T(0) + v T_{at} - T(v), \quad (4)$$

$$E_{bvac}(v) = T(-v) + v T_{at} - T(0). \quad (5)$$

Thus the energy E_{bad}/E_{bvac} is needed to remove one by one the ad/vacancy atoms from the surface to the vacuum. The adiabatic removal of an atom from the surface can be seen as a two-step process, where vacancy-adatom formation is followed by removal of the adatom. Note that the five energies defined earlier are not independent from each other:

$$E_{va} = E_{ad} + E_{vac}, \quad (6)$$

$$E_{va} + E_{bad} = E_{bvac}. \quad (7)$$

The energetic results for each surface and vacancy size are summarized in Table 2 together with the structural deformation d_{ef} . The deformation d_{ef} is measured as the distance of an atom to its initially ideal crystal position in percentage of the nearest neighbor distance and corrected for periodic boundary conditions, where Table 2 shows the maximal values of d_{ef} .

From our findings, E_{va} is the most important value for the prediction of possible surface reconstruction, since it is the minimum energy that has to be compensated by the interaction between the adsorbate species (C_{60} in our case) and the surface to allow for vacancy formation. In particular, the dissociation energy D for removing C_{60} from the surface vacancy —also called the adsorption energy— needs to be even larger than the sum of E_{va} and D for the case of a clean surface so as to make the reconstruction energetically favorable. From the E_{va} values of Table 2 we observe that, for a single atom vacancy, Be (2.09 eV) is more stable than Al (1.6 eV), which is in turn more stable than Au (1.11 eV). The enhanced stability of Be could be explained by its higher melting point (1551 K) compared to Al (933 K), and Au (1338 K).⁷⁸ However, by this line of reasoning, Au should be more stable than Al,

which is not reflected by our results. In contrast, they suggest that surface reconstruction should proceed more easily in gold than in aluminum or beryllium. However, E_{vac} is only slightly smaller for Au than for Al and only for $v = 1$ and $v = 3$, whereas for $v = 7$ Au gains stability against Al in terms of E_{vac} . The reversed stability order of E_{va} compared to melting points originates mainly from the adatom formation energies E_{ad} for $v \leq 3$. Au is likely to overtake Al in stability for larger surface reconstructions ($v > 7$), in accordance with the melting points of the metals. E_{va} is, as expected, not directly proportional to v , as fewer bonds-to-neighbors have to be broken for the removal of more and more atoms. An increase by a factor of 1.8-2.2 is observed when going from one- to three-atom vacancies, and of 2.3-3.2 from one- to seven-atom vacancies. Thus, after the first three atoms are removed, removing any additional atom comes at a significantly reduced energy expense (*circa* 147, 258, and 278 meV atom⁻¹ for Al, Au, and Be, respectively). It should be noted that in the case of septuple vacancy pits, the $5 \times 5 \times (6 + L_z)$ unit-cell might be too small and interactions between neighboring pits could influence our results, since only two rows of atoms separate the craters. In these cases results should be taken as indicating trends rather than as absolute values.

Table 2: Energies of vacancy-, adatom-, and vacancy-adatom formation as well as structural deformation for single, triple, and septuple atom pits.

	v	$E_{va}/$ eV	$E_{ad}/$ eV	$E_{vac}/$ eV	$E_{bad}/$ eV	$E_{bvac}/$ eV	$d_{ef}/\%$
Al	1	1.60	0.91	0.69	2.83	4.42	18.7
	3	3.11	1.59	1.52	9.61	12.72	52.3
	7	3.70	2.23	1.48	23.91	27.61	70.5
Au	1	1.11	0.53	0.58	3.20	4.31	3.0
	3	2.49	1.30	1.20	9.91	12.40	9.6
	7	3.52	1.76	1.76	24.39	27.91	7.5

Be	1	2.09	0.84	1.25	3.01	5.11	7.1
	3	3.77	1.40	2.36	10.16	13.92	8.0
	7	4.88	2.13	2.74	24.84	29.72	12.8

A deep inspection of the formation energy values encompassed by Table 2 unveils that the two contributions to E_{va} (E_{ad} and E_{vac}) carry almost equal weights for Au. In the case of Al the adatom formation energy dominates, whereas in case of Be it is the vacancy formation energy. Regardless of the case, E_{bad} and E_{bvac} scale with v . Single-atom vacancy binding energies E_{bvac} are larger than cohesive energies for the three metals. This means that the removal of a single atom from the surface takes more energy than removing an atom from the perfect bulk. Thus, indirectly, E_{bvac} carries information about the stability of a material against sputtering, in a better fashion than the cohesive energy. As far as deformation is concerned, Al deforms rather dramatically whereas Au and Be vary much less. In general, the deformation increases from the fixed bottom layers to the top layer and towards the vacancies or adatoms.

The computed vacancy and adatom formation energies appear to be in accord with previous computed values in the literature. In particular, the E_{va} formation energy of 1.72 eV reported by Stumpf and Scheffler for Al(111)⁷⁷ is composed of $E_{vac} = 0.67$ eV and $E_{ad} = 1.05$ eV. Less agreement is found with DFT calculations within the Local Density Approximation (LDA) which yielded an E_{vac} energy of 0.36 eV for Al(111),⁷⁹ and 0.83 eV for Au(111).¹⁴ The value for Al(111) seems especially low since another study within the Generalized Gradient Approximation (GGA) and LDA by Kiejna *et al.*⁸⁰ yielded values of 0.61 and 0.66 eV, respectively, again in perfect agreement with our value of 0.69 eV. Previous studies reported E_{vac} for Au to be between 0.77 to 0.82 eV,⁸¹ in accordance with Li *et al.*,¹⁴ but slightly larger than our value of 0.58 eV. Other theoretical and experimental values for Au showed values between 0.82 and 0.93 eV, thus again slightly higher.⁸² We examined whether this

discrepancy of E_{vac} for a single atom was due to our vdW correction, yet the estimate without Grimme's correction yielded a similarly low value of 0.55 eV.

C₆₀ Adsorption

In view of the high electron affinity of C₆₀, a metal→C₆₀ charge transfer is expected, which leads to ionic binding in addition to possible covalent bonds. The above mentioned dissociation energy D is defined as:

$$D = T(C_{60}) + T(-v) - T(-v, C_{60}), \quad (8)$$

where $T(C_{60})$ is the total energy of C₆₀ in vacuum (cell size dimensions of 20 Å) and $T(-v, C_{60})$ the total energy of the surface with v vacancies and C₆₀ adsorbed upon. Results for D are collected in in Table 3 with (D_v) and without (D) vdW correction, together with the available literature values. The energies without vdW correction were obtained for geometries that were optimized including this correction. For all considered materials and surface structures we obtain a high value of D_v around or larger than 2 eV. The winner is gold with a particularly high adsorption energy whereas Al and Be share the second rank. In a previous DFT study Tang *et al.* obtained, without applying any dispersion correction, adsorption energies of 2.07, 2.33, and 2.56 eV for single, triple, and septuple atom vacancies, respectively, as compared to a value of 1.2 eV for a dense monolayer of C₆₀ at clean Au(111).¹⁵ Note that in this work a denser fullerene monolayer was used, and, consequently, the reduced adsorption energies may well be the result of steric repulsions between fullerenes. Other DFT works report adsorption strengths of the order of 1.9-2.2 eV for fullerene adsorbed on clean gold,^{16, 83} and classical force field models depicted binding strengths of 1.26 and 3.12 eV for C₆₀ on surface reconstructed grooves and dimples, respectively.⁸⁴

In any case we see that, by comparing D_v and D of Table 3, vdW dispersion seems to play a major role in the attachment of fullerenes to metal surfaces, as had also been found for similar systems such as graphene.⁸⁵ For example, C_{60} was found to adsorb on Au(111) with a hexagon parallel to the surface over an *hcp* three-fold hollow site,²⁵ with a primarily covalent bond of 1.27 eV strength, and a charge transfer of 0.2 e , according to DFT calculations without vdW description. A subsequent DFT study including vdW¹⁷ showed that adsorption is dominated by dispersive forces, yet bonding remained covalent in nature. The optimized structure, close to the presently obtained one, implies a binding to the *fcc* three-fold hollow site with binding strengths in the range of 1.71-2.97 eV depending on the method for dispersion correction. We also found that optimization without the Grimme correction resulted in rather small adsorption energies of 0.16 eV for clean Al and 0.07 eV for clean Be with C_{60} locating far away from the surface. A previous DFT study of $C_{60}/\text{Au}(111)$ without accounting for dispersion obtained a similarly low binding energy of 0.18 eV.⁸⁶ However, the C_{60} desorption temperature of both Au(111) and Al(111) lies around 700 K, suggesting a strong covalent bonding with the surface.^{16, 43}

As a general trend vacancies strongly enhance the adsorption energy. It first increases with the vacancy number v , but it may well happen that at some point the extension of the pit exceeds that of C_{60} . Consequently, D_v decreases again from $v = 3$ to $v = 7$ for Al and Be.

Table 3: Dissociation energies (equivalent to the adsorption energy of C_{60} at the substrate) with (D_v) vdW corrections, without them (D) and from literature (D_l). Also given are the Bader charge transfer q_{CT} , and the number of covalent bonds n_{CB} .

	Al(111)				Au(111)				Be(001)			
v	0	1	3	7	0	1	3	7	0	1	3	7

D_v/eV	1.99	3.97	4.28	3.44	3.39	4.21	4.94	5.20	2.45	3.69	4.21	3.58
D/eV	-0.15	1.57	1.81	0.40	-0.28	0.34	0.29	-0.23	0.47	1.53	1.69	0.44
D_I/eV	1.37 ¹⁴	2.34 ¹⁴	-	-	1.2 ¹⁵	2.07 ¹⁵	2.33 ¹⁵	2.56 ¹⁵	-	-	-	-
q_{CT}/e	-2.3	-4.2	-4.1	-5.2	-0.08	-0.2	-0.18	-0.11	-4.8	-4.3	-5.2	-6.1
n_{CB}	6	6	4	6	0	0	0	0	6	6	9	9

A Bader electron density analysis reveals large charge transfer from Al and Be to C_{60} .⁸⁷ It increases dramatically with ν , up to 6 electrons for $\nu = 7$, that are transferred from Be to C_{60} , although the electron affinity of isolated C_{60} is only positive up to C_{60}^{2-} .⁸⁸ A completely different behavior is found for Au which retains the electrons, so the charge transfer is limited to 0.1-0.2 e . Previous ultraviolet photoelectron spectroscopy experiments estimated a charge transfer from gold to C_{60} of $1\pm 0.2 e$. This exceeds the value predicted by our as well as other DFT calculations, by a large margin.^{25, 40} This result is likely to arise from the well-known excessive delocalization trend exhibited by GGA functionals which, among other effects, leads to too small band gaps in metal oxides and too large magnetic coupling constants in magnetic oxides and related system.⁸⁹ In other words, GGA tend to make everything too metallic. All these deficiencies are corrected when using hybrid functionals as shown by Moreira et al. for NiO ⁸⁹ and more recently by Hofmann et al.⁹⁰ for organic molecules on Ag(111) and also by Della Sala et al.⁹¹ for SAM on Au(111). Clearly, hybrid density functional methods cannot be applied to the very large systems studied in the present work. On the other hand, except for the magnitude of the charge transfer between the fullerene and the metallic surfaces, the overall physical picture will remain the same.

The true locations of charge accumulation and depletion are resolved in Charge Density Difference (*CDD*) maps, see Figure 1. Again the bonding mechanism at the Au

surface is completely different than the bonding at Al and Be. For Au depletion regions that resemble well-localized p -orbitals (blue lobes) are found, extending far inside the Au surface. The charge is transferred to the red-green clouds that might be interpreted as covalent bonds, as also found by Hamada *et al.* and Hinterstein *et al.* by DFT-based CDD plots showing the directional character of C-Au bonds.^{11, 17} Interestingly, the CDD plots do not show all these features without taking vdW into account.²⁵ We also looked at the Electron Localization Functions (*ELF*) and found no apparent covalent bonds for C₆₀ on Au in contrast to C₆₀ on either Al or Be, where clear signatures of covalent bonding appear at the places of charge accumulation between C₆₀ and the respective surface (Figure 2). In the case of Be, two C atoms are seen to share bonds to one surface atom. For Al, in contrast, every C atom is clearly bonded to one specific surface atom. This results in different optimized geometries because the bottom hexagon of C₆₀ resides on top of an Al atom but in the center of three Be atoms, see Figures 1e, 1f. The number of covalent bonds n_{CB} observed from ELF is given in Table 3 as well. The deeper the vacancies get, the deeper the fullerene dives into the surface, and different atoms become available for covalent bonding. The ELF covalent regions of the clean surface are much smaller than the ones in the presence of vacancies, mirroring the corresponding difference in D .

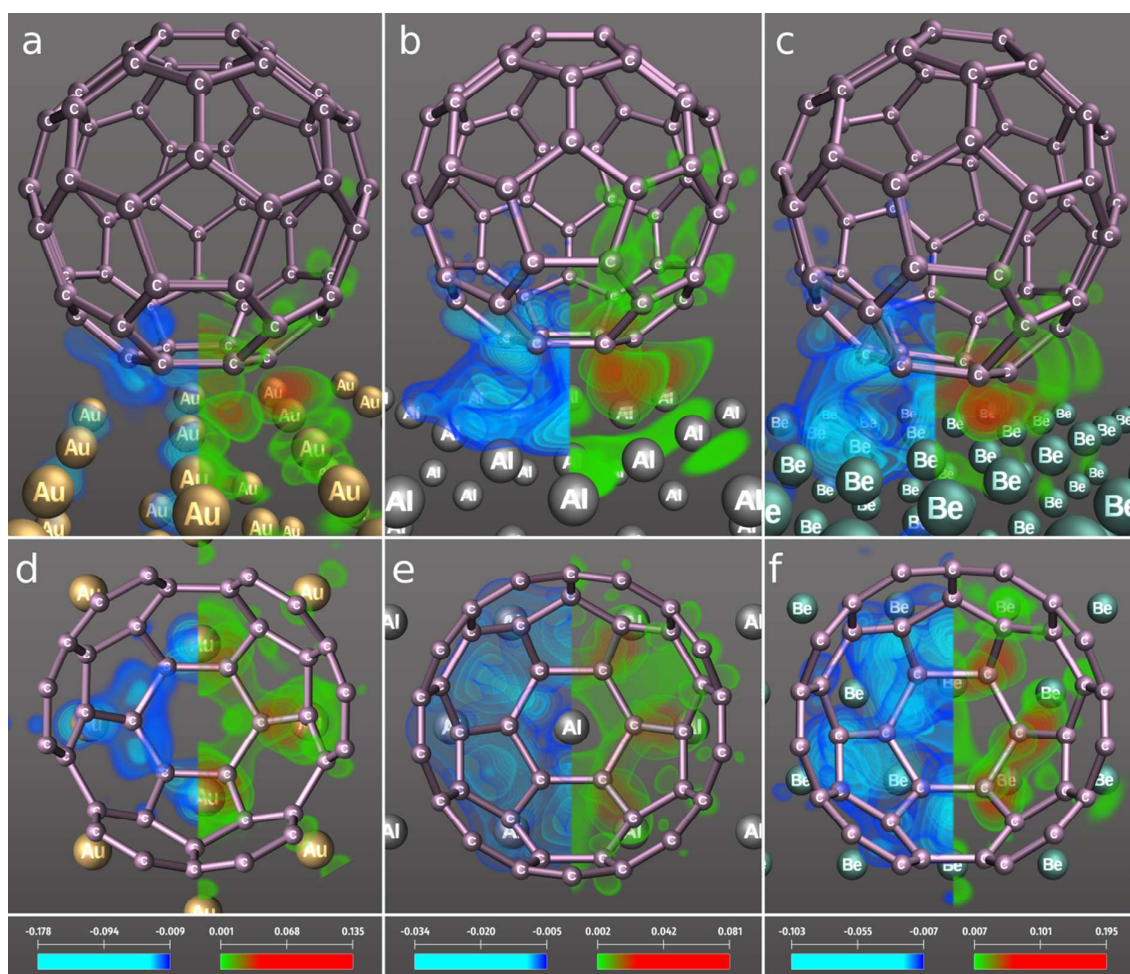


Figure 1: Front (a, b, c) and top (d, e, f) views of CDD volume renderings of regions with charge accumulation (green→red = low→high) and depletion (blue→light blue = low→high) due to adsorption of C₆₀ for clean surfaces of Au (a, d), Al (b, e), and Be (c, f). For the sake of clarity very small charge differences are omitted.

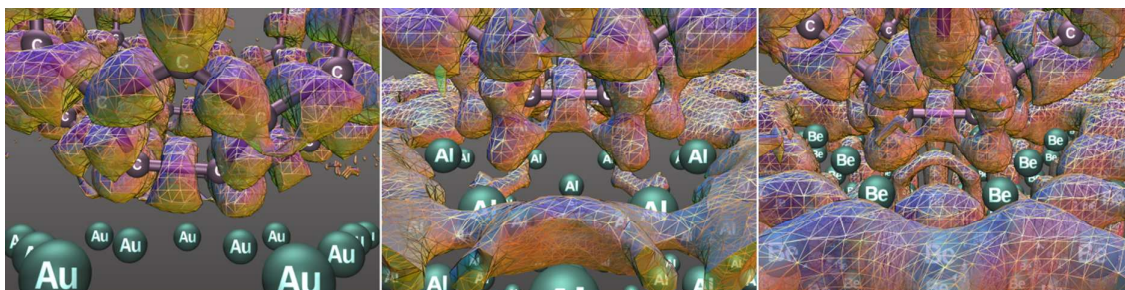


Figure 2: ELF contours for C_{60} on Au(111), Al(111) and Be(0001) surfaces with single-atom vacancies; left, middle and right panels, respectively. The contours correspond to high values of ELF (0.7) to highlight the formation of covalent electron pairs for Al and Be, in contrast to Au.

The total Density Of States (*DOS*) for C_{60} adsorbed on Al system is projected on the Al atoms in Figure 3a and compared with the DOS of a pristine Al surface. Note that the amplitudes for Al+ C_{60} without and with the seven-atom vacancy were resized to meet the amplitudes of the pristine Al DOS at low energy. Small changes appear both below and above the Fermi level (E_F) upon absorption of C_{60} , where the discrete states of C_{60} are superposed with the quasi-continuum of the surface. The DOS is smeared out due to the seven-atom vacancy and marginally by the presence of C_{60} . The same comparison for Au yields a similar picture with a much lower degree of smearing, while for Be the DOS is relatively unaffected by adsorption of C_{60} and vacancy formation. These observations are in accordance with the fact that Al deforms in response to vacancy formation and C_{60} adsorption more than the other two metals (see also Table 2).

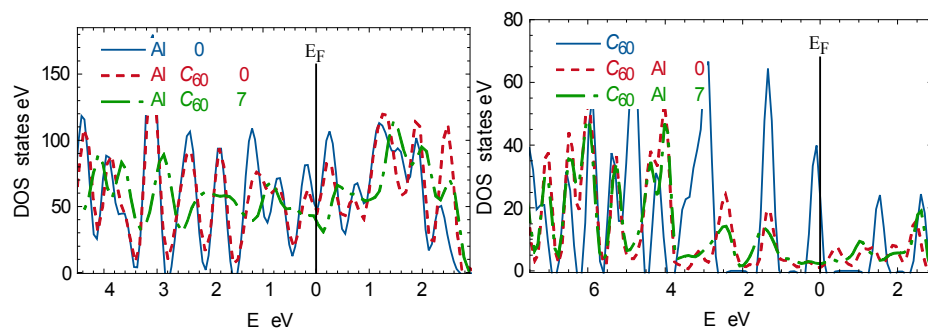


Figure 3: DOS of aluminum in $C_{60}+Al(v)$ compared to the clean Al surface (a) and DOS of carbon in $C_{60}+Al(v)$ compared to C_{60} in vacuum (b).

The scaled DOS projected on carbon atoms is shown in Figure 3b; compared to C_{60} in vacuum the C_{60} states when adsorbed on Al are shifted to lower energies by ~ 1 eV. Furthermore, in the vicinity of E_F the sharp peaks of the molecule are tremendously smeared out, yielding metallic behavior, and a small part of the Lowest Unoccupied Molecular Orbital (*LUMO*) is shifted below E_F , in accordance with previous DFT calculations.²⁵ This effect is stronger when C_{60} is adsorbed to a vacancy than on the clean surface. Largely similar observations are made for the cases of Au and Be. The findings are consistent with previous Scanning Tunneling Spectroscopy (*STS*) experiments on Au(110), which revealed that a significant fraction of C_{60} *LUMO* broadens and shifts downwards towards the Fermi level.⁸

Discussion

We first discuss fullerene adsorption induced vacancy formation. Upon adsorption, the dissociation energy D_v is released, and this can give rise to vacancy formation, since $D_v(v) > E_{va}(v)$ for all structures considered here except for septuple-atom vacancies for Al and Be. However, other adsorption energy dissipation channels exist. A better suited criterion to determine whether a vacancy formation is thermodynamically allowed is that the energy D_v on a vacancy must surpass that on the clean surface plus the vacancy-atom formation energy: $D_v(v) > D_v(0) + E_{va}(v)$. This ensures the adsorption-on-a-vacancy state to be the ground state, being of higher stability than the adsorption on the pristine surface. The latter,

more strict criterion is only fulfilled for Al(111) single-atom vacancies, where a total energy gain of 0.38 eV is recorded. However, the missing energy for the other structures is not very high (0.29 eV for Au and 0.85 eV for Be in the case of the single-atom vacancy) and therefore could easily be supplied, for instance, by addition of the adatom nearby C_{60} , or by forming surface dimers, or even larger clusters. In addition, adsorbate location at step edges could gain extra energy,^{12, 77} given the enhanced adsorption-ability of surface under-coordinated metal atoms located at edges between terraces.⁹² Besides, the small energy cost could be thermally supplied. Overall, adsorption of C_{60} reduces the cost of vacancy formation compared to pristine surfaces. This clearly points at the formation of surface metal vacancies that follow the pattern of C_{60} adsorbates. The concept is backed up by STM experiments which showed bright and dim C_{60} on Au(111), where dim molecules were identified to reside on top of multiatom vacancies.¹⁰ This is an example of how the adsorption of a C_{60} monolayer yielded a periodic ordering of adsorption-induced vacancies on the surface.

The conditions for C_{60} CSA are more difficult to assess. One can propose a *Gedankenexperiment* involving a metal surface with already well-separated vacancies and a temperature large enough to allow for C_{60} diffusion over vacancy-free surface areas. Thus, the first deposited C_{60} can move freely on the clean surface until it finds a vacancy. A recent study estimated an activation energy of 13 meV for single fullerene diffusion on Au(111);⁸³ such a small activation energy would allow C_{60} to easily find vacancies, supporting the CSA feasibility. Since the binding energy on the vacancy is by 1-2 eV larger than on the clean surface, the C_{60} will remain anchored there unless the temperature is too high. A second C_{60} has two possible fates. Either it moves nearby to the first C_{60} and initializes cluster nucleation, releasing a few hundreds of meV,⁹³ or it finds an unoccupied vacancy, releasing a much higher margin of energy. From an energetic point of view there would be a temperature window, where nucleation is suppressed because the binding to other C_{60} is not strong

enough, while simultaneously C_{60} forms stable bonds to vacancies. The above-introduced competing process of induced vacancy formation could, however, complicate this picture. We conclude that with accurate temperature control, the self-assembly on pre-structured template surfaces —containing surface vacancies— could be controlled, leading to user-defined patterns of adsorbate molecules, given that adsorption-induced vacancy formation is energetically unfavorable, such as on Au(111) and Be(0001).

Previous STM experiments of $C_{60}/Au(111)$ at RT assisted by DFT calculations also revealed vacancies as preferred bonding sites.¹⁵ At 46 K C_{60} molecules seem to attach to the elbow sites of the Au(111) herringbone reconstruction. When annealing to RT these sites are vacated, and nucleation at step edges occurs without vacancy formation. When starting directly at RT, Tang *et al.* found individual molecules at elbow sites and further cluster nucleation in between them upon further deposition, whereas at low temperature clusters only nucleated around single molecules adsorbed at elbow sites. This controversy led the authors to argue that vacancies form below C_{60} to stabilize its adsorption at RT. The hypothesis was supported by a C_{60} height of 6.2 Å at 46 K while at RT C_{60} lies 2.2 Å deeper. This *sinking* is in agreement with the adsorption over seven-atom pits, and demonstrates that C_{60} can be safely stored over vacancies at RT, supporting the idea of the CSA process that will be necessary for envisaged nanodevices. XRD studies also showed surface reconstruction with pit formation to accommodate C_{60} on Au(110),¹¹ and on herringbone Au(111).⁹ The latter displayed C-Au distances of 2.49 Å with a C_{60} hexagon facing the single-atom vacancy, close to our value of 2.33 Å, indicating a mixed covalent/ionic bonding.

As far as aluminum is concerned, the Al(111) surface also reconstructs under a compressed C_{60} overlayer.^{12, 42-44} Stengel *et al.* proposed that two Al adatoms from single-atom vacancies under two out of three adsorbed C_{60} form a dimer that stays in the interstitial region between C_{60} molecules, further stabilizing the system.¹² The structure naturally

explains why one out of three C_{60} protrudes from the surface. The authors gave adsorption energies ranging 0.98-1.38 eV, yet not accounting for vdW forces, and estimated a total energy gain due to the reconstruction of $0.8/3 = 0.27$ eV per C_{60} molecule. In another related study¹⁴ LDA DFT calculations yielded adsorption energies on pristine surfaces of 1.37, 1.25, and 1.52 eV for Al, Au, and Ag, respectively. On vacancies the adsorption energies increased to 2.34, 2.69, and 2.61 eV, respectively. The authors also contemplated structures where vacancy atoms occupy the free space in between C_{60} . Using the unreconstructed surface as energy reference, the adsorption energies are 1.40, 1.35, and 1.59 eV. Here the energy needed to create a vacancy is accounted for, and still these adsorption energies are by 0.10, 0.03, and 0.07 eV larger than the adsorption energies found on clean surfaces. This study suggests C_{60} -induced vacancy formation on all considered surfaces, and is fully compatible with our results for aluminum.

No literature values were found for beryllium which turned out to be most resistant with respect to vacancy formation among the three metals investigated in this work. The stability of Be surface could be useful for the CSA process.

Conclusions

We studied the energetic criteria for vacancy formation and fullerene adsorption on gold, aluminum and beryllium surfaces. To this end we employed density functional theory calculations taking van der Waals interactions into account. We found that the cost for vacancy formation increases in the order $Au < Al < Be$. A strong adsorption of C_{60} is found for all metals, surpassing dissociation energies of 2 eV. Adsorption on surface vacancies is enhanced compared to pristine surfaces, so that C_{60} molecules might occupy user-defined patterns of vacancies (*vacancy patterning*). On the other hand, the adsorption energy on an Al vacancy is higher than for adsorption on the pristine surface plus the vacancy costs; only a slight endothermicity is found for Au and Be. This suggests the possibility of *patterning*

vacancies when adsorbing C_{60} on these surfaces. The computational results are backed up with available experimental evidence, and future applications are envisaged for such a patterning in nanodevices. The fact that Be is less susceptible to surface vacancy formation than Al should be kept in mind when comparing the sputtering properties of these metals.

Acknowledgements

Part of this work was supported by the Austrian Ministry of Science BMWF as part of the UniInfrastrukturprogramm of the Focal Point Scientific Computing at the University of Innsbruck and funded by the Austrian Science Fund (FWF) DK+ project Computational Interdisciplinary Modeling, W1227-N16. This work was also supported by the Spanish MICINN grant CTQ2012-30751, and, in part, by the Generalitat de Catalunya (grants 2009SGR1041 and XRQTC). F.V. thanks the MINECO for the postdoctoral *Juan de la Cierva* and *Ramón y Cajal* grants (JCI-2010-06372, RYC-2012-10129), F.I. acknowledges additional funding through the 2009 ICREA Academia award for excellence in university research. F.H. acknowledges support from the Tennessee NSF-EPSCoR Grant TN-SCORE (NSF EPS 1004083). Support by the European Commission under the Contract of Association between EURATOM and the Austrian Academy of Sciences within the framework of the European Fusion Development Agreement is also acknowledged.

References

1. K. D. Schierbaum, T. Weiss, E. U. T. van Veizen, J. F. J. Engbersen, D. N. Reinhoudt and W. Göpel, *Science*, 1994, **265**, 1413-1415.
2. E. Menard, M. A. Meitl, Y. Sun, J.-U. Park, D. J.-L. Shir, Y.-S. Nam, S. Jeon and J. A. Rogers, *Chem. Rev.*, 2007, **107**, 1117-1160.
3. I. Díez-Pérez, M. Luna, F. Teherán, D. F. Ogletree, F. Sanz and M. Salmeron, *Langmuir*, 2004, **20**, 1284-1290.
4. S. M. Kozlov, F. Viñes and A. Görling, *Adv. Mat.*, 2011, **23**, 2638-2643.
5. M. Garnica, D. Stradi, S. Barja, F. Calleja, C. Diaz, M. Alcamí, N. Martín, A. L. Vazquez de Parga, F. Martín and R. Miranda, *Nat. Phys.*, 2013, **9**, 368-374.

6. P. Vettiger, G. Cross, M. Despont, U. Drechsler, U. Durig, B. Gotsmann, W. Haberle, M. A. Lantz, H. E. Rothuizen, R. Stutz and G. K. Binnig, *IEEE Trans. Nanotechnol.*, 2002, **1**, 39-55.
7. G. N. Vayssilov, Y. Lykhach, A. Migani, T. Staudt, G. P. Petrova, N. Tsud, T. Skála, A. Bruix, F. Illas, K. C. Prince, V. Matolin, K. M. Neyman and J. Libuda, *Nat. Mater.*, 2011, **10**, 310-315.
8. J. K. Gimzewski, S. Modesti and R. R. Schlittler, *Phys. Rev. Lett.*, 1994, **72**, 1036-1039.
9. X. Torrelles, M. Pedio, C. Cepek and R. Felici, *Phys. Rev. B*, 2012, **86**, 075461.
10. L. Tang, Y. Xie and Q. Guo, *J. Chem. Phys.*, 2011, **135**, 114702.
11. M. Hinterstein, X. Torrelles, R. Felici, J. Rius, M. Huang, S. Fabris, H. Fuess and M. Pedio, *Phys. Rev. B*, 2008, **77**, 153412.
12. M. Stengel, A. D. Vita and A. Baldereschi, *Phys. Rev. Lett.*, 2003, **91**, 166101.
13. R. Felici, M. Pedio, F. Borgatti, S. Iannotta, M. Capozzi, G. Ciullo and A. Stierle, *Nat. Mater.*, 2005, **4**, 688-692.
14. H. I. Li, K. Pussi, K. J. Hanna, L. L. Wang, D. D. Johnson, H. P. Cheng, H. Shin, S. Curtarolo, W. Moritz, J. A. Smerdon, R. McGrath and R. D. Diehl, *Phys. Rev. Lett.*, 2009, **103**, 056101.
15. L. Tang, X. Zhang, Q. Guo, Y.-N. Wu, L.-L. Wang and H.-P. Cheng, *Phys. Rev. B*, 2010, **82**, 125414.
16. C. T. Tzeng, W. S. Lo, J. Y. Yuh, R. Y. Chu and K. D. Tsuei, *Phys. Rev. B*, 2000, **61**, 2263-2272.
17. I. Hamada and M. Tsukada, *Phys. Rev. B*, 2011, **83**, 245437.
18. J. A. Gardener, G. A. D. Briggs and M. R. Castell, *Phys. Rev. B*, 2009, **80**, 235434.
19. C. Rogero, J. I. Pascual, J. Gomez-Herrero and A. M. Baro, *J. Chem. Phys.*, 2002, **116**, 832-836.
20. M. Pedio, R. Felici, X. Torrelles, P. Rudolf, M. Capozzi, J. Rius and S. Ferrer, *Phys. Rev. Lett.*, 2000, **85**, 1040-1043.
21. S. Modesti, S. Cerasari and P. Rudolf, *Phys. Rev. Lett.*, 1993, **71**, 2469-2472.
22. Y. Kuk, D. K. Kim, Y. D. Suh, K. H. Park, H. P. Noh, S. J. Oh and S. K. Kim, *Phys. Rev. Lett.*, 1993, **70**, 1948-1951.
23. R. J. Wilson, G. Meijer, D. S. Bethune, R. D. Johnson, D. D. Chambliss, M. S. de Vries, H. E. Hunziker and H. R. Wendt, *Nature*, 1990, **348**, 621-622.
24. X. Zhang, W. He, A. Zhao, H. Li, L. Chen, W. W. Pai, J. Hou, M. M. T. Loy, J. Yang and X. Xiao, *Phys. Rev. B*, 2007, **75**, 235444.
25. L.-L. Wang and H.-P. Cheng, *Phys. Rev. B*, 2004, **69**, 165417.
26. X. Lu, M. Grobis, K. H. Khoo, S. G. Louie and M. F. Crommie, *Phys. Rev. B*, 2004, **70**, 115418.
27. M. Kiguchi, K.-i. Iizumi, K. Saiki and A. Koma, *Appl. Surf. Sci.*, 2003, **212–213**, 101-104.
28. M. Pedio, K. Hevesi, N. Zema, M. Capozzi, P. Perfetti, R. Gouttebaron, J. J. Pireaux, R. Caudano and P. Rudolf, *Surf. Sci.*, 1999, **437**, 249-260.
29. J. Weckesser, J. V. Barth and K. Kern, *Phys. Rev. B*, 2001, **64**, 161403.
30. C. Liu, Z. Qin, J. Chen, Q. Guo, Y. Yu and G. Cao, *J. Chem. Phys.*, 2011, **134**, 044707-044706.
31. X. Torrelles, V. Langlais, M. De Santis, H. C. N. Tolentino and Y. Gauthier, *J. Phys. Chem. C*, 2010, **114**, 15645-15652.
32. M. Sogo, Y. Sakamoto, M. Aoki, S. Masuda, S. Yanagisawa and Y. Morikawa, *J. Phys. Chem. C*, 2010, **114**, 3504-3506.

33. T. Orzali, D. Forrer, M. Sambri, A. Vittadini, M. Casarin and E. Tondello, *J. Phys. Chem. C*, 2007, **112**, 378-390.
34. M. Casarin, D. Forrer, T. Orzali, M. Petukhov, M. Sambri, E. Tondello and A. Vittadini, *J. Phys. Chem. C*, 2007, **111**, 9365-9373.
35. W. W. Pai, H. T. Jeng, C. M. Cheng, C. H. Lin, X. Xiao, A. Zhao, X. Zhang, G. Xu, X. Q. Shi, M. A. Van Hove, C. S. Hsue and K. D. Tsuei, *Phys. Rev. Lett.*, 2010, **104**, 036103.
36. A. Tamai, A. P. Seitsonen, F. Baumberger, M. Hengsberger, Z. X. Shen, T. Greber and J. Osterwalder, *Phys. Rev. B*, 2008, **77**, 075134.
37. L.-L. Wang and H.-P. Cheng, *Phys. Rev. B*, 2004, **69**, 045404.
38. A. Ogawa, M. Tachibana, M. Kondo, K. Yoshizawa, H. Fujimoto and R. Hoffmann, *J. Phys. Chem. B*, 2003, **107**, 12672-12679.
39. R. Nouchi and I. Kanno, *J. Appl. Phys.*, 2003, **94**, 3212-3215.
40. B. W. Hoogenboom, R. Hesper, L. H. Tjeng and G. A. Sawatzky, *Phys. Rev. B*, 1998, **57**, 11939-11942.
41. R. Fasel, P. Aebi, R. G. Agostino, D. Naumović, J. Osterwalder, A. Santaniello and L. Schlapbach, *Phys. Rev. Lett.*, 1996, **76**, 4733-4736.
42. M. K. J. Johansson, A. J. Maxwell, S. M. Gray, P. A. Brühwiler, D. C. Mancini, L. S. O. Johansson and N. Mårtensson, *Phys. Rev. B*, 1996, **54**, 13472-13475.
43. A. J. Maxwell, P. A. Brühwiler, D. Arvanitis, J. Hasselström, M. K. J. Johansson and N. Mårtensson, *Phys. Rev. B*, 1998, **57**, 7312-7326.
44. A. J. Maxwell, P. A. Brühwiler, S. Andersson, D. Arvanitis, B. Hernnäs, O. Karis, D. C. Mancini, N. Mårtensson, S. M. Gray, M. K. J. Johansson and L. S. O. Johansson, *Phys. Rev. B*, 1995, **52**, R5546-R5549.
45. J. G. Hou, J. Yang, H. Wang, Q. Li, C. Zeng, H. Lin, W. Bing, D. M. Chen and Q. Zhu, *Phys. Rev. Lett.*, 1999, **83**, 3001-3004.
46. Y. Z. Li, M. Chander, J. C. Patrin, J. H. Weaver, L. P. F. Chibante and R. E. Smalley, *Phys. Rev. B*, 1992, **45**, 13837-13840.
47. J. V. Barth, H. Brune, G. Ertl and R. J. Behm, *Phys. Rev. B*, 1990, **42**, 9307-9318.
48. T. Allmers and M. Donath, *New J. Phys.*, 2009, **11**, 103049.
49. G. Li, V. Shrotriya, J. Huang, Y. Yao, T. Moriarty, K. Emery and Y. Yang, *Nat. Mater.*, 2005, **4**, 864-868.
50. T. M. Clarke and J. R. Durrant, *Chem. Rev.*, 2010, **110**, 6736-6767.
51. G. Federici, *Phys. Scr.*, 2006, **2006**, 1.
52. T. Maihom, I. Sukuba, R. Janev, K. Becker, T. Märk, A. Kaiser, J. Limtrakul, J. Urban, P. Mach and M. Probst, *Eur. Phys. J. D*, 2013, **67**, 1-5.
53. G. Kresse and J. Furthmüller, *Phys. Rev. B*, 1996, **54**, 11169-11186.
54. G. Kresse and J. Furthmüller, *Comp. Mat. Sci.*, 1996, **6**, 15-50.
55. G. Kresse and J. Hafner, *Phys. Rev. B*, 1993, **47**, 558-561.
56. G. Kresse and J. Hafner, *Phys. Rev. B*, 1994, **49**, 14251-14269.
57. J. P. Perdew, K. Burke and M. Ernzerhof, *Phys. Rev. Lett.*, 1996, **77**, 3865-3868.
58. P. E. Blöchl, *Phys. Rev. B*, 1994, **50**, 17953-17979.
59. S. Grimme, *J. Comp. Chem.*, 2006, **27**, 1787-1799.
60. M. Amft, L. Sébastien, O. Eriksson and N. V. Skorodumova, *J. Phys.: Condens. Matter*, 2011, **23**, 395001.
61. M.-T. Nguyen, C. A. Pignedoli, M. Treier, R. Fasel and D. Passerone, *Phys Chem Chem Phys*, 2010, **12**, 992-999.
62. W. Benger, G. Ritter and R. Heinzl, in *4th High-End Visualization Workshop, Obergurgl, Tyrol, Austria, June 18-21, 2007*, Berlin, Lehmanns Media-LOB.de, 2007, ch. 26-39.

63. A. Kaiser, O. Ismailova, A. Koskela, S. E. Huber, M. Ritter, B. Cosenza, W. Benger, R. Nazmutdinov and M. Probst, *J. Mol. Liq.*, 2014, **189**, 20-29.
64. M. Ritter, *CCT-TR*, 2009, **13**, 1-67.
65. Mineralogy Database, <http://www.webmineral.com/>, Accessed 10/08, 2013.
66. R. Gaudoin, W. M. C. Foulkes and G. Rajagopal, *J. Phys.: Condens. Matter*, 2002, **14**, 8787.
67. C. J. Fall, N. Binggeli and A. Baldereschi, *Phys. Rev. B*, 1998, **58**, R7544-R7547.
68. H. L. Skriver and N. M. Rosengaard, *Phys. Rev. B*, 1992, **46**, 7157-7168.
69. J. Schöchlin, K. P. Bohnen and K. M. Ho, *Surf. Sci.*, 1995, **324**, 113-121.
70. B. Chan and W.-L. Yim, *J. Chem. Theory Comput.*, 2013, **9**, 1964-1970.
71. P. A. Anderson, *Phys. Rev.*, 1959, **115**, 553-554.
72. C. J. Fall, N. Binggeli and A. Baldereschi, *Phys. Rev. B*, 2000, **61**, 8489-8495.
73. R. J. Needs and M. Mansfield, *J. Phys.: Condens. Matter*, 1989, **1**, 7555.
74. A. Hao and Y. Zhu, *J. Appl. Phys.*, 2012, **112**, 023519-023514.
75. M. Y. Chou, P. K. Lam and M. L. Cohen, *Phys. Rev. B*, 1983, **28**, 4179-4185.
76. P. Stoltze, *J. Phys.: Condens. Matter*, 1994, **6**, 9495.
77. R. Stumpf and M. Scheffler, *Phys. Rev. B*, 1996, **53**, 4958-4973.
78. K. Barbalace, Periodic Table of Elements. EnvironmentalChemistry.com. 1995 - 2014., <http://environmentalchemistry.com/yogi/periodic/>, Accessed 03/14, 2014.
79. H. M. Polatoglou, M. Methfessel and M. Scheffler, *Phys. Rev. B*, 1993, **48**, 1877-1883.
80. A. Kiejna, *Phys. Rev. B*, 2003, **68**, 235405.
81. P. A. Korzhavyi, I. A. Abrikosov, B. Johansson, A. V. Ruban and H. L. Skriver, *Phys. Rev. B*, 1999, **59**, 11693-11703.
82. T. Korhonen, M. J. Puska and R. M. Nieminen, *Phys. Rev. B*, 1995, **51**, 9526-9532.
83. A. V. Akimov, C. Williams and A. B. Kolomeisky, *J. Phys. Chem. C*, 2012, **116**, 13816-13826.
84. R. J. Baxter, P. Rudolf, G. Teobaldi and F. Zerbetto, *ChemPhysChem*, 2004, **5**, 245-248.
85. S. M. Kozlov, F. Viñes and A. Görling, *J. Phys. Chem. C*, 2012, **116**, 7360-7366.
86. E. Abad, J. Ortega, Y. J. Dappe and F. Flores, *Appl. Phys. A*, 2009, **95**, 119-124.
87. W. Tang, E. Sanville and G. Henkelman, *J. Phys.: Condens. Matter*, 2009, **21**, 084204.
88. W. H. Green, S. M. Gorun, G. Fitzgerald, P. W. Fowler, A. Ceulemans and B. C. Titeca, *J. Phys. Chem.*, 1996, **100**, 14892-14898.
89. I. de P. R. Moreira, F. Illas and R. L. Martin, *Phys. Rev. B*, 2002, **65**, 155102.
90. O. T. Hofmann, V. Atalla, N. Moll, P. Rinke and M. Scheffler, *New J. Phys.*, 2013, **15**, 123028.
91. F. D. Sala, E. Fabiano, S. Laricchia, S. D'Agostino and M. Piacenza, *Int. J. Quantum Chem.*, 2010, **110**, 2162-2171.
92. F. Vines, J. R. B. Gomes and F. Illas, *Chem. Soc. Rev.*, 2014.
93. S. Zöttl, A. Kaiser, M. Daxner, M. Goulart, A. Mauracher, M. Probst, F. Hagelberg, S. Denifl, P. Scheier and O. Echt, *Carbon*, 2014, **69**, 206-220.

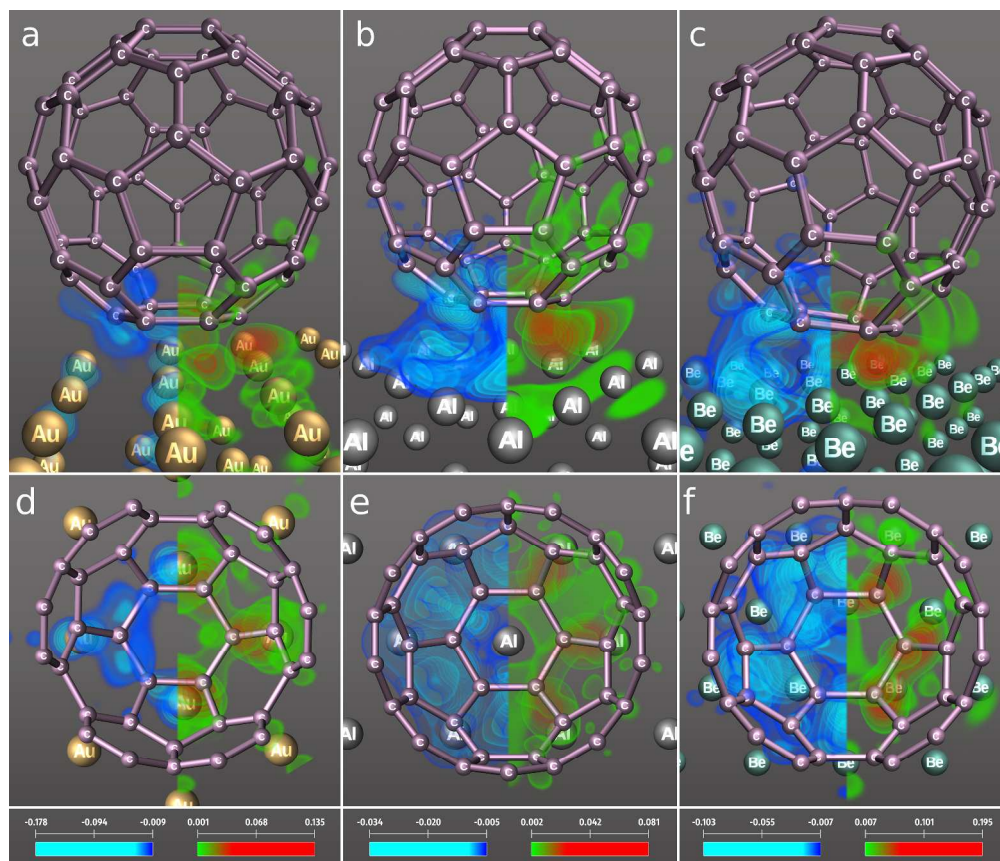


Figure 1: Front (a, b, c) and top (d, e, f) views of CDD volume renderings of regions with charge accumulation (green→red = low→high) and depletion (blue→light blue = low→high) due to adsorption of C⁶⁰ for clean surfaces of Au (a, d), Al (b, e), and Be (c, f). For the sake of clarity very small charge differences are omitted.

1499x1281mm (72 x 72 DPI)

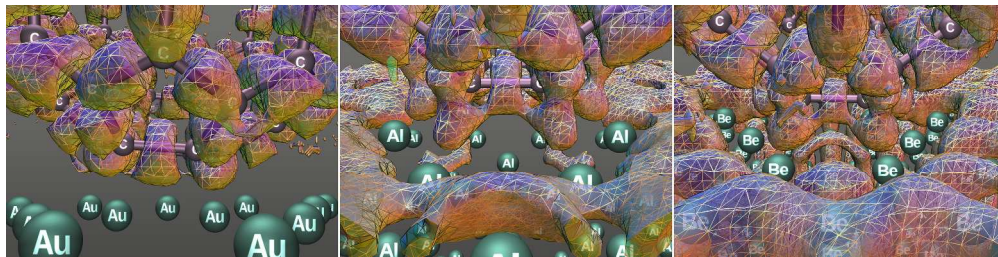
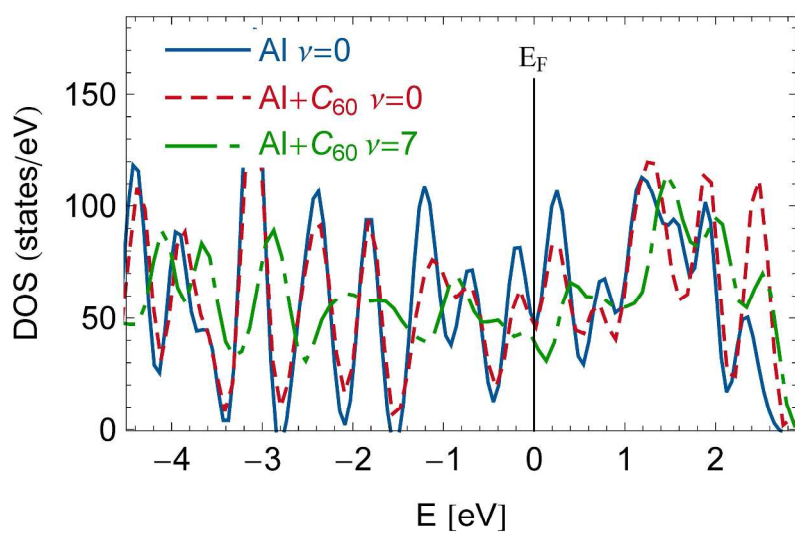
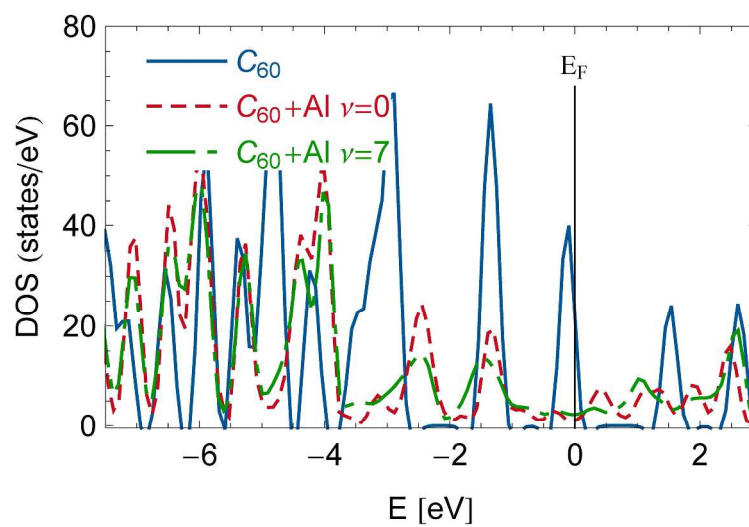


Figure 2: ELF contours for C_{60} on Au(111), Al(111) and Be(0001) surfaces with single-atom vacancies; left, middle and right panels, respectively. The contours correspond to high values of ELF (0.7) to highlight the formation of covalent electron pairs for Al and Be, in contrast to Au.
1424x356mm (72 x 72 DPI)



DOS of aluminum in $C_{60}^+Al(\nu)$ compared to the clean Al surface (a) and DOS of carbon in $C_{60}+Al(\nu)$ compared to C_{60} in vacuum (b).

279x361mm (300 x 300 DPI)



279x361mm (300 x 300 DPI)